Mutations in tetratricopeptide repeat domain 7A (*TTC7A*) are associated with combined immunodeficiency with dendriform lung ossification but no intestinal atresia

Bo Ngan[a]*, Daniele Merico[b], Nufar Marcus[c,d], Vy H.D. Kim[e], Julia Upton[e], Andrea Bates[e], Joanne Herbrick[b], Thomas Nalpathamkalam[b], Bhooma Thiruvahindrapuram[b], Peter Cox[c,d], and Chaim M. Roifman[e]

ABSTRACT

Introduction: Genetic aberrations associated with combined immunodeficiency have been increasingly identified in the past two decades. Yet, there are still 30% of these patients with unidentified genetic cause.

Methods: We employed whole genome sequencing to identify the genetic defect leading to combined immunodeficiency. Thymus, gut, and lung tissues were studied using hematoxylin and eosin staining as well as immunohistochemistry.

Results: We identified 2 deleterious mutations in the *TTC7A* gene. Surprisingly, the patient did not have intestinal atresia but suffered repeated infections as well fatal pneumonitis. Dendriform lung ossification developed, which was unique to this case. The patient had typical presentation of combined immunodeficiency including profound lymphopenia, markedly reduced in-vitro response to mitogens, as well as low TRECS. Serum immunoglobulins were also markedly reduced.

Conclusion: Mutations in the *TTC7A* gene can cause combined immunodeficiency with no intestinal atresia and predispose to lung ossification.

Statement of novelty: *TTC7A* mutations can cause profound immunodeficiency without multiple intestinal atresia. We report here for the first time that this defect is associated with dendriform lung ossification.

[a] The Department of Paediatric Laboratory Medicine, The Hospital for Sick Children and The University of Toronto, Toronto, ON, Canada; [b] The Centre for Applied Genomics, The Hospital for Sick Children and The University of Toronto, Toronto, ON, Canada; [c] Department of Critical Care Medicine, The Hospital for Sick Children and The University of Toronto, Toronto, ON, Canada; [d] Department of Pediatrics Kipper Institute of Allergy and Immunology, Schneider Children Medical Center of Israel, Tel Aviv, Israel; [e] Division of Immunology and Allergy, The Canadian Centre for Primary Immunodeficiency, The Jeffrey Modell Research Laboratory for the diagnosis of Primary Immunodeficiency, The Hospital for Sick Children and The University of Toronto, Toronto, ON, Canada

*Corresponding author: Bo Ngan, (email: bo-yee.ngan@sickkids.ca).
The first two authors contributed equally.

Introduction

Combined immunodeficiency (CID) defines a group of patients with profound T-cell deficiency who, unlike patients with typical severe combined immunodeficiency (SCID), have circulating T cells with various levels of dysfunction (Roifman et al. 2012). Over the past two decades the genetic aberrations underlining CID have been increasingly identified, including Zap-70 deficiency, CD25 deficiency, and others (Arpaia et al. 1994; Sharfe et al. 1997; Roifman et al. 2000). Still, in 20%–30% of patients with CID the molecular basis of their disease remains poorly defined.

One type of combined immunodeficiency was found to be associated with multiple intestinal atresias (MIA) (OMIM 2431500). This condition is usually severe and affects multiple sections of the small and large bowel (Mishalany and Der Kaloustian 1971; Guttman et al. 1973; Arnal-Monrea et al. 1983; Moreno et al. 1990; Walker et al. 1993; Gungor et al. 1995; Rothenberg et al. 1995; Moore et al. 1996; Gahukamble et al. 2002; Gahukamble and Gahukamble 2002; Bilodeau et al. 2004; Cole et al. 2010). In spite of attempts to surgically correct these lesions, outcome generally has been poor and the condition remains fatal in most affected individuals. The pathogenesis of the intestinal lesions remains unclear, although autoimmune mechanisms have been proposed, mainly because of the associated T-cell dysfunction. Most cases of MIA have been sporadic but some familial cohorts have been reported (Mishalany and Der Kaloustian 1971; Guttman et al. 1973; Arnal-Monrea et al. 1983; Moreno et al. 1990; Walker et al. 1993; Gungor et al. 1995; Rothenberg et al. 1995; Moore et al. 1996; Gahukamble et al. 2002; Gahukamble and Gahukamble 2002; Bilodeau et al. 2004; Cole et al. 2010).

Recently, genetic aberrations in the tetraticopeptide repeat domain 7A (*TTC7A*) gene were identified in MIA patients by using whole exome sequencing (Chen et al. 2013; Samuels et al. 2013; Bigorgne et al. 2014). However, the function of *TTC7A* remains poorly understood.

Multiple tetratricopeptide repeat (TPR) domains in this protein have been recognized as protein–protein interaction domains potentially involved in cellular processes such as phosphate turnover, cell cycle, and subcellular localization.

Spontaneous mutations in the mouse *TTC7A* ortholog *Ttc7* lead to distinct phenotypes with severe skin manifestations as well as hematopoietic features, but unlike humans there is little involvement of the gut or the immune system (Beamer et al. 1995; Abernethy et al. 2000; White et al. 2004; Helms et al. 2005; Takabayashi and Katoh 2005; White et al. 2005; Takabayaski et al. 2007).

We report here for the first time a case of CID with unique features. By using whole genome sequencing on this patients DNA, 2 mutations in *TTC7A* were identified. Like other cases of CID this patient had chronic diarrhea, but uniquely the patient suffered dendriform pulmonary ossification and had no evidence of intestinal atresias.

Methods

Immunoglobulin and specific antibody

Serum concentrations of immunoglobulins were measured using nephelometry. Serum IgE concentration was measured using radioimmunoassay with the IgE PRIST kit (Pharmacia Diagnostics, Que.). Levels of serum antibodies to tetanus were measured using enzyme-linked immunosorbent assay, and polio antibody titres were determined using complement fixation.

T and B cell proliferative responses

Lymphocyte proliferative responses to mitogens, including phytohemagglutinin (PHA) and anti-CD3 antibodies, and to a panel of recall antigens (including candida, tetanus, herpes zoster, and cytomegalovirus) were determined using thymidine incorporation at day 3 or day 6. All assays were performed in triplicate and were compared with simultaneously stimulated randomized normal controls.

Whole genome sequencing

The whole genome of the subject was sequenced using the Complete Genomics platform. The concentration of genomic DNA sample was measured using PicoGreen in triplicate and about 11 μg of DNA was submitted to Complete Genomics for whole genome sequencing. Complete Genomics employs high-density DNA nanoarrays that are concatamers of mate pair reads, each approximately 500 bp long. Base identification is performed using a nonsequential, unchained read technology known as combinatorial probe-anchor

ligation (cPAL). Each mate pair includes 35 nucleotides (nt) of genomic DNA sequence as well as adaptor sequences required for cPAL sequencing; the average mate gap length is 300 bp.

Small variants (SNV, insertions, deletions, block substitutions) as well as copy number variants were called as part of computer-generated imagery (CGI) sequencing service, using the CGI pipeline version 2.2.

Small variant quality filters

Variants were primarily quality filtered according to CGI's default quality filters, based on the variant allele fraction quality score. More stringent quality filters were defined by (*i*) requiring the number of supporting reads (totalReadCount) to be ≥5; (*ii*) requiring the estimated ploidy to be 2 for autosomes as well as for the X chromosome (the sample being female and thus having two copies of the X chromosome); (*iii*) requiring the equal allele fraction quality score also to be passed (score ≥40 for heterozygous, score ≥20 for homozygous calls), which penalizes variants deviating from a diploid model; (*iv*) requiring the ratio between reads supporting the alternate and the reference to be ≥0.35 for heterozygous variants and ≥0.80 for homozygous variants. All variants were considered, but variants passing the higher quality filters were given priority.

Small variant re-annotation pipeline

Annovar (Wang et al. 2010) and custom scripts were used to re-annotate variants (data processed in January 2014).

Variants were mapped to gene coding exons using Annovar and the RefSeq database (based on the hg19 assembly). In the presence of overlapping genomic regions (e.g., 3′ untranslated region [3′ UTR] of gene A overlapping with coding exon of gene B), Annovar follows predefined annotation precedence (e.g., coding exon has precedence over 3′ UTR).

Annovar was used to classify variants as synonymous, missense, stop-loss, stop-gain, splicing (defined as overlapping the 2 intronic bp preceding the intron–exon junction), frameshift insertion/deletions/substitutions, and nonframeshift insertion/deletions/substitutions. Alternate allele frequencies were added by Annovar using the 1000 Genome database (version:

phase 1 release version 3, called from Nov. 11, 2010, alignment), National Heart Lung and Blood Institute–Exome Sequencing Project (NHLBI–ESP) (version: esp6500si) and the Complete Genomics diversity panel; for 1000 Genome and NHLBI-ESP, allele frequencies were imported for the global dataset as well as specific ethnic subgroups. Annovar was also used to map variants to dbSNP137and ClinVar entries. In particular, dbSNP was mapped matching genomic coordinates and allele and was also based only on coordinate overlap; the common polymorphism subset of dbSNP entries was additionally mapped as separate annotation fields to help remove common variants. SIFT, PolyPhen2 (HVAR version), and Mutation Assessor scores, which predicted the impact of missense variants on protein sequence, were imported from the LJB database (version 2) using Annovar. PhyloP nucleotide-level conservation scores derived from placental mammal and 100 vertebrate genome sequence alignments were imported from the corresponding UCSC tracks using custom scripts. Finally, gene–phenotype associations based on human disorders or mouse knockout or other transgenic experiments were imported using custom scripts (data downloaded and processed in August 2013).

Small variant prioritization

Variant frequency tiers were defined by requiring variants to have alternate alleles below given frequency thresholds (5%, 1%) in all the allele frequency databases used. Variants were predicted to be damaging based on the following rules: (*a*) all stop-gain, splicing, and frameshift; (*b*) missense variants with placental mammal Phylop ≥1 (or 100-vertebrate PhyloP ≥1.5) and at least one of the following five criteria satisfied: (*i*) SIFT score <0.05, (*ii*) PolyPhen2 HVAR score ≥0.95, (*iii*) mutation assessor score ≥2, (*iv*) placental mammal PhyloP score ≥2.40, and (*v*) 100-vertebrate PhyloP score ≥4; (*c*) nonframeshift insertions/deletions/substitutions with placental mammal Phylop ≥1.5 (or 100-vertebrate PhyloP ≥2.5) and not mapped to dbSNP common by exact matching or coordinate overlap. High quality, 5% rare variants matching ClinVar entries with pathogenic significance were extracted and assessed inspecting frequency and associated disorder.

All high quality, 1% rare, coding and predicted damaging variants were assigned to the following groups for more detailed investigation: (*i*) all homozygous, recessive mode of inheritance; (*ii*) potential compound heterozygous (i.e., when more than one variant satisfying the criteria above could be found per

gene), recessive mode of inheritance; and (*iii*) all heterozygous, dominant mode of inheritance, potentially de-novo. X-linked transmission from the mother to the male affected offspring was not possible given the proband's female gender. Variants were additionally tiered based on the gene–phenotype associations: 2683 genes were found implicated in immune phenotypes in human or mouse, of which 436 had a dominant mode of inheritance in humans.

CNV annotation pipeline

Copy number gains and losses reported in "snvSegmentsDipliodBeta" were separately annotated for frequency, based on 50% reciprocal overlap with CNV called in 54 unrelated samples from the Complete Genomic diversity panel (pipeline version 2.2).

Pathology

The infant patient underwent thymus, gastric, duodenal, transverse colon, descending colon, and rectal biopsies for the investigation of immunodeficiency and diarrhea. After the patient's death, parental consent was granted to perform an autopsy limited to the chest and abdomen. The histopathology in the thymus and the patient's age matched normal thymus control; the gastrointestinal tract and lungs were also analyzed. All histochemical and immunohistochemistry stains were performed on formalin-fixed paraffin embedded tissues. Three to five μm tissue slides for microscopy were stained with hematoxlyn and eosin (H&E) after deparaffinization for light microscopy. The monoclonal antibodies used were commercially available. Antibodies against CD3, 4, 8, Mib-1, cytokeratin, and smooth muscle actin were supplied in prediluted forms by Ventana (Roche diagnostics, Tucson, AZ). For the other antibodies used, they were supplied and diluted as follows: CD133, 1/400 (AbCam, Cambridge, MA); CD163, 1/100 (Leica Bioscience Ltd., Newcastle, UK); TTF-1, 1/100 (Leica Bioscience Ltd.); Fox P3, 1/20 (Bioscience, San Diego, CA); Osteonectin, 1/50 (Biogenex, San Ramon, CA); and Cleaved Caspase3, 1/200 (Cell Signaling Technology, Danvers, MA). With the exception of cytokeratin immunostain, where protease pretreatment using enzyme and reagents from Ventana were applied, antigen retrieval procedures by heat treatment of deparaffinized tissue slides in buffered citrate solution were used. The sensitivity of the antibody binding detection was enhanced by either using Ultraview Horse Radish Peroxidase (HRP) linked multimer or a combination of biotinylated anti-antibody with Strepavidin-HRP reagents (both were from Ventana), and the antibody binding was visualized by the chromogen reaction with hydrogen peroxide and diazobenzidine. These tissue sections were counterstained with hematoxylin. Immunostains were performed with an automated immunostainer (model BenchMark XT, Ventana, Tucson, AZ).

Results

Case report

A female infant was born small for gestational age (2.46 kg) at 36 weeks to a father of Sudanese descent and a Caucasian mother. She had feeding difficulties, vomiting, diarrhea, and failure to thrive during the first four weeks of life. She suffered repeated episodes of sepsis with *Staphylococcus aureus, Escherichia coli*, and *Serratia marcescens*. At the early age of 3 months she was found to have lymphopenia. At the age of 5 months she was transferred to another hospital and again had repeated episodes of sepsis with *Serratia marcescens*, *streptococcal pneumoniae*, and *Staphylococcus aureus*. She was then transferred to our institution for further evaluation of her immunity. The patient developed pneumonitis due to para influenza virus and her respiratory status deteriorated gradually. In spite of maximal support treatment in the pediatric intensive care unit she died of hypoxic cardiac arrest at the age of 1 year.

Microarray analysis, karyotype, and chromosome breakage studies were normal. Genetic testing showed no abnormalities in RMRP, CD25, CD3ε, CD3δ, STAT1, IL-7Rα, IL-10, IL-10Rα, and IL-10Rβ.

Immune evaluation

Immune evaluation revealed a low lymphocyte count with lymphocyte immunophenotyping showing $CD3^+$ 791 cells/μL, $CD4^+$ 365 cell/μL, $CD8^+$ 265 cell/μL, and $CD56^+$ 17 cell/μL cells. In vitro responses to PHA and anti-CD3 antibody stimulation were markedly reduced at <40% and <10% of controls, respectively. T-cell repertoire was also abnormal. The $CD4^+$ cell compartment showed reduced representation of the Vβ3, Vβ9, and Vβ14 families, whereas Vβ5,3, Vβ13,2, and Vβ20 were overrepresented. Repertoire skewing was more prominent in $CD8^+$ cells, whereby Vβ3, Vβ9, Vβ14,

Vβ17, and Vβ23 families were underrepresented, with overrepresentation of Vβ21.3 only (Figure 1).

These results predicted impaired function of the thymus. We performed a thymus biopsy that showed a small and depleted gland. Most Hassall's corpuscles were small and poorly formed and their total number was markedly diminished when compared with a control (11 vs. 57 per field), thus clearly suggesting a primary immunodeficiency (Figures 2A and 2B). Corticomedullary demarcation was also compromised, with

a reduced number of thymocytes in the cortical regions. Cytokeratin staining confirmed the rarity of Hassall's corpuscles and their immature nature (Figure 2C). Immunohistochemistry for CD3, CD4, and CD8 appear to show positive staining, but overall numbers were reduced in full agreement with H&E staining (Figures 2D and 2E). Remarkably, the number of FOXP3^{+} regulatory cells was also drastically reduced in the patient's thymus (Figure 2F). In support of the notion of a dysfunctional thymus, T-cell receptor excision circle (TREC) levels, which represent new thymus
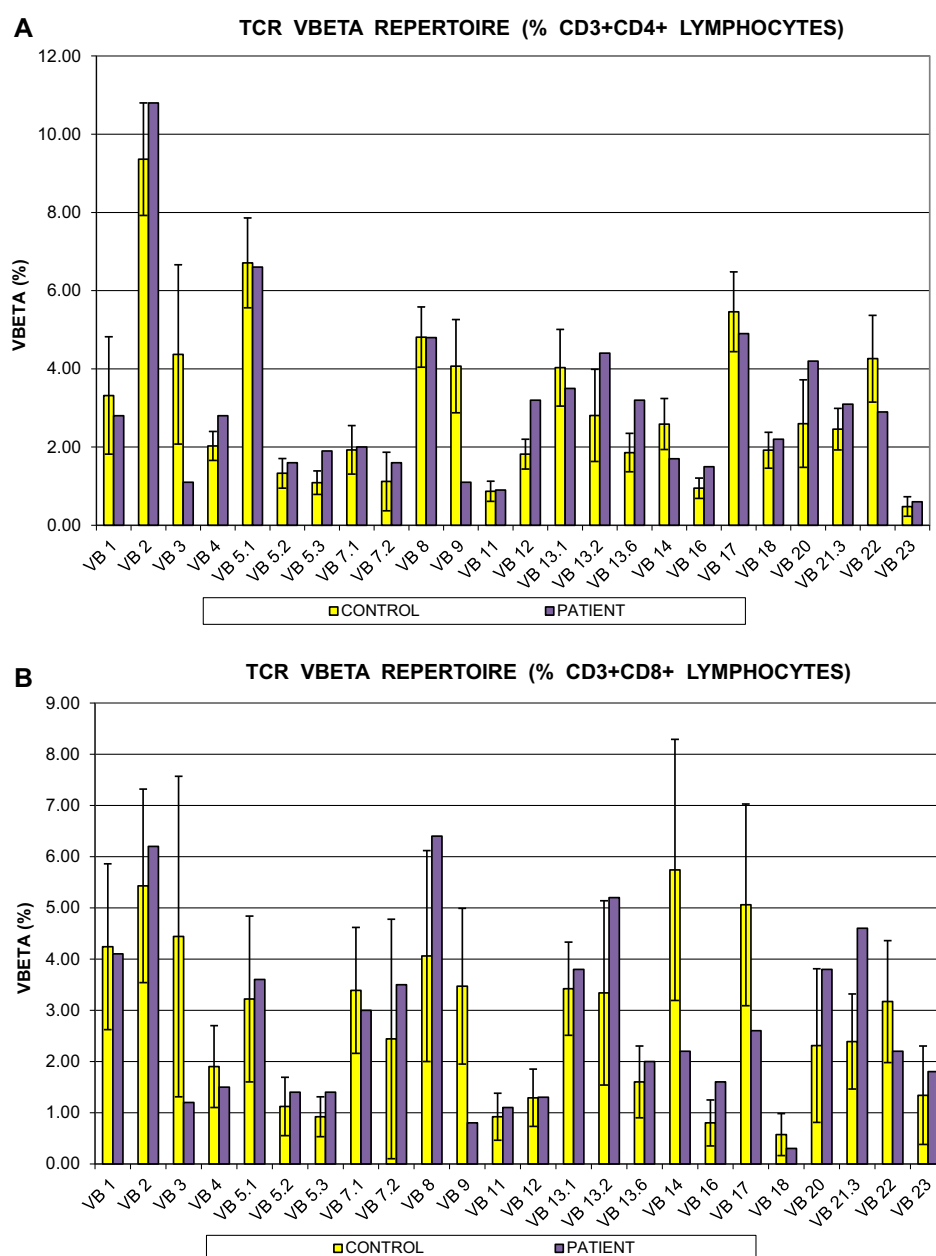

Figure 1: Flow cytometry analyses of the T-cell repertoire in patient's blood. Each Vβ subtype are expressed as percent of CD3^{+} CD4^{+} lymphocytes (A) and CD3^{+} CD8^{+} lymphocytes (B).

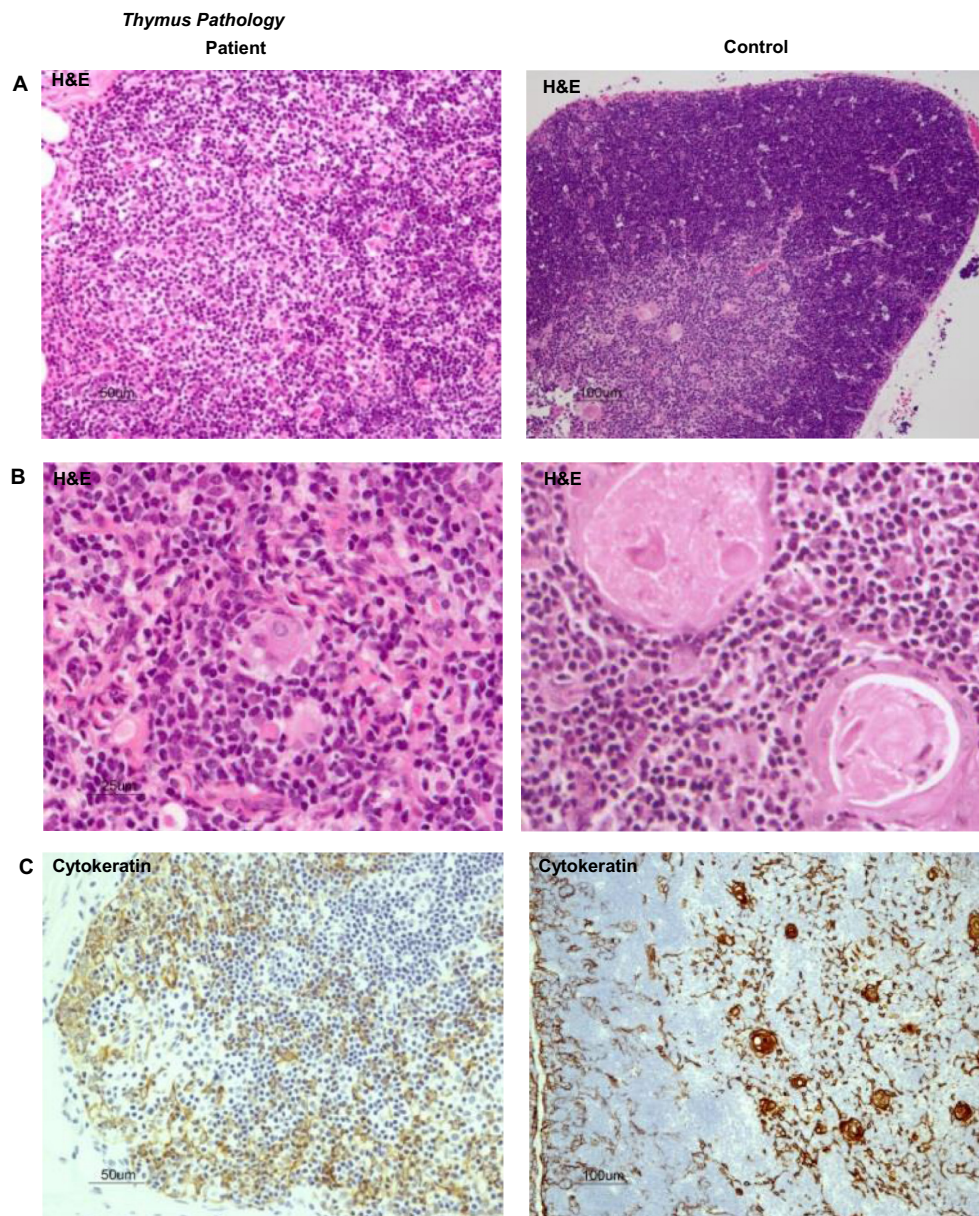**Thymus Pathology**

Patient | Control

Figure 2: Histopathological and immunopathologcal features between patient thymus (left column) and that of normal age matched thymus control is shown. H&E, marked cortical lymphoid depletion with poor demarcation of cortico-medullary junction (A). H&E, abortive formation Hassall corpuscles; only sporadic epitheliod epithelial cells clusters are evident (B). Cytokeratin immunostain shows scattered thymic epithelial cells without formation of cortical thymic reticulum meshwork or Hassall corpuscles in the medulla (C). CD4 (D) and CD8 (E); both (D) and (E) show marked reduction of CD4 and CD8 T-cells in both cortex and medulla, respectively. FOX P3[+] T-regulatory cells are also markedly reduced compared with the normal control (F).

emigrants, were reduced (275 ± 120 in three different determinants).

Immunoglobulins were all low (IgG < 0.6 g/L, IgA <0.2 g/L, and IgM < 0.2 g/L) and specific antibody production in response to vaccination was undetectable.

Lung pathology

Evaluation of the autopsy lung pathology revealed diffuse alveolar damage and severe interstitial pulmonary fibrosis with honeycomb transformation of the pulmonary parenchyma (Figure 3A). There was marked reduction of alveoli and all were structurally
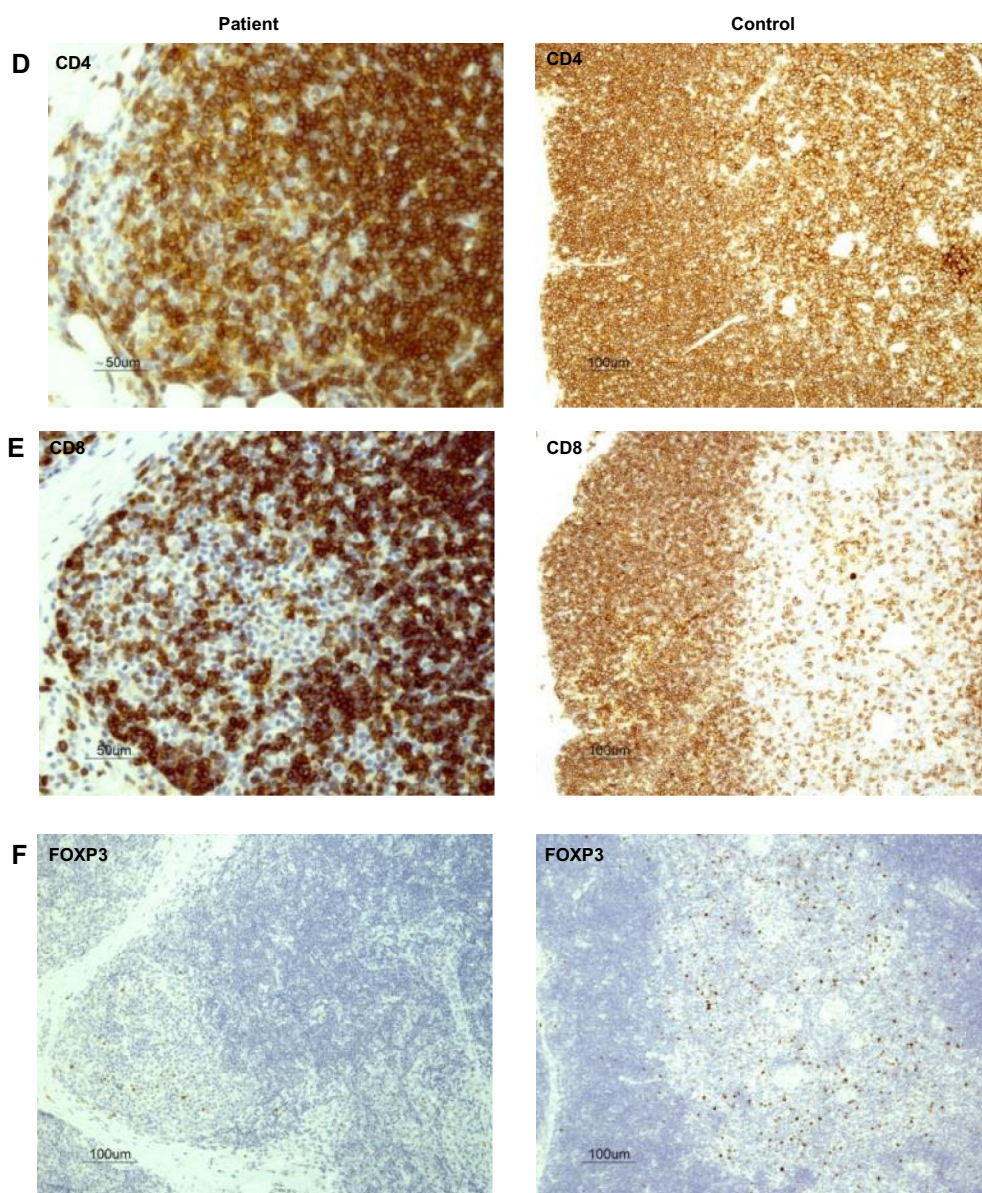
Patient	Control

Figure 2: Continued

remodeled into small round air filled microcysts that were lined with low cuboidal type-2 pneumocytes. These cells were found positive for pan cytokeratin and TTF-1 by immunostaining (Figures 3B and 3C). In addition, diffuse micro-dendriform pulmonary ossification was present. Dendriform networks of thin spicules of metaplastic osseous tissues were formed within the abnormal thick and fibrotic interalveolar septae (Figure 3A). The metaplastic osseous tissues arose within the stroma that contained smooth muscle actin expressing myofibroblasts (Figure 3D). Osteoblasts were associated with the bone spicules, and many of them showed active remodeling by osteoclasts (Figures 4A and 4B). It appeared that this osteogenic activity was in its initial stages of bone marrow development. Within the

fibrotic stroma there were clear foci of hematopoeisis, such as microscopic aggregates of para-trabecular progenitor myeloid, erythroid, and megakaryocytic cells (Figures 4C and 4D). Analyses of the cell types within the microenvironment of the fibrotic interalveolar pulmonary interstium, which showed osteogenesis, demonstrated a close association between smooth muscle actin-positive myofibroblasts and macrophages that expressed the activation antigen CD163 (Figures 5A and 5B respectively). Immunostaining for the presence of osteonectin, one of the major noncollagenous proteins of bone associated with osteogenic differentiation from myofibroblasts, showed that it was expressed in the dendriform bone spicules (Figure 6A) as well as in the myofibroblasts in the vicinity of the
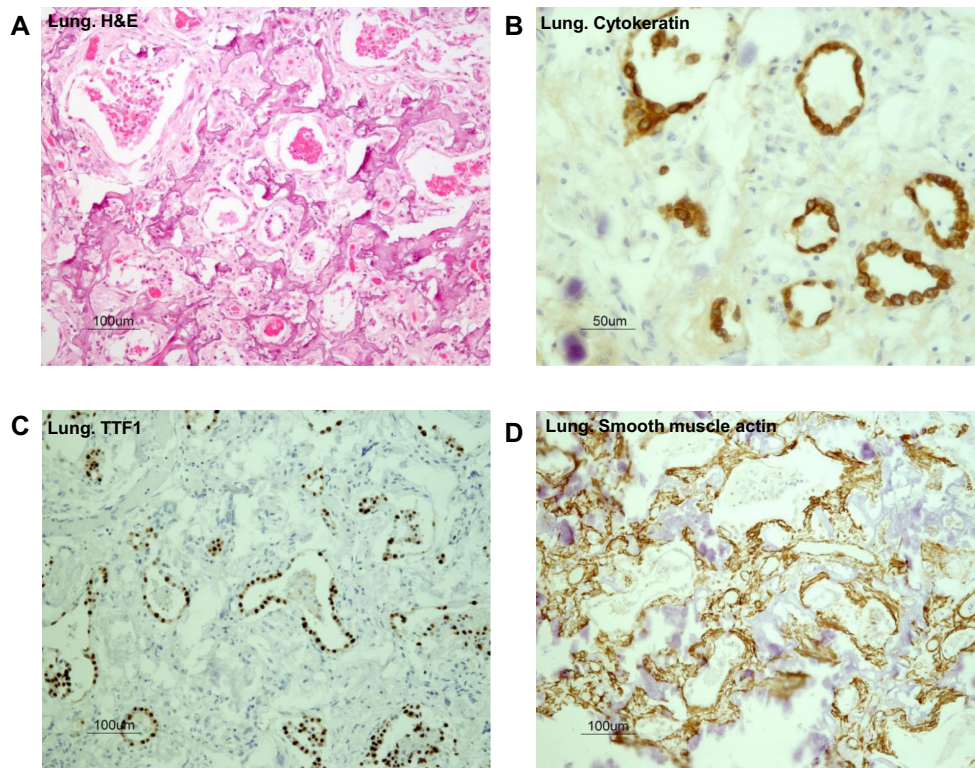
Figure 3: Dendriform ossification within honeycomb lung fibrosis. Histopathological features of severe lung fibrosis with honeycomb formation where alveolar spaces are transformed into small air cysts lined exclusively by cuboidal type 2 pneumocytes. In addition, within the widened interalveolar septum, spicules of bone (dendriform bone) are formed in a diffuse manner (H&E) (A). Cytokeratin positive cuboidal cells lined the air cysts (B) and they are of pulmonary origin as they express TTF1 (C). The widening of the interalveolar septum is due to the abnormal and exuberant proliferation of myofibroblasts as they are known to express smooth muscle actin (D).

bone spicules. Immunostaining for T cells with CD3 showed that this microenvironment was devoid of T cells (Figure 6B).

There were no histological features of bronchiolitis obliterans and no residual infiltrates of chronic inflammatory cells were seen within the fibrotic pulmonary interstitium. No viral cytopathic changes were found and stains for fungi and bacteria and immunostains for adenovirus, cytomegalovirus, and respiratory syncytial virus were all negative. DNA amplification by polymerase chain reaction detected parainfluenza A (consistent with patient's history).

Gut pathology

Biopsy of the duodenum showed moderate partial villous atrophy with paucity of inflammatory cells in the lamina propria. There was no evidence of tufting

and there were no cytoplasmic changes consistent with microvillous inclusion disease. Periodic acid – Schiff stain demonstrated a well-preserved brush border. The colonic biopsy showed marked mucosal injury with regenerative mucosal glandular alterations. Enterocyte apoptosis was seen predominantly in the enterocytes in the basal regions of the crypts (Figure 7). Apoptosis was evidenced by expression of cleaved caspase 3 (Figures 8A and 8B) as well as structural anomalies, such as increased transit amplifying zone characterized by Mib-1 positive cells (Figure 8C) and abnormal location of CD133 positive crypt stem cells (Figure 8D). Paneth cells and neuroendocrine cells were present.

Genetic analysis

To identify the underlining genetic cause of this disorder we employed whole genome sequencing. The

A — Lung osteoids with osteoblasts

B — Lung osteoids with osteoclasts

C — Lung. erythropoiesis, osteoid stroma

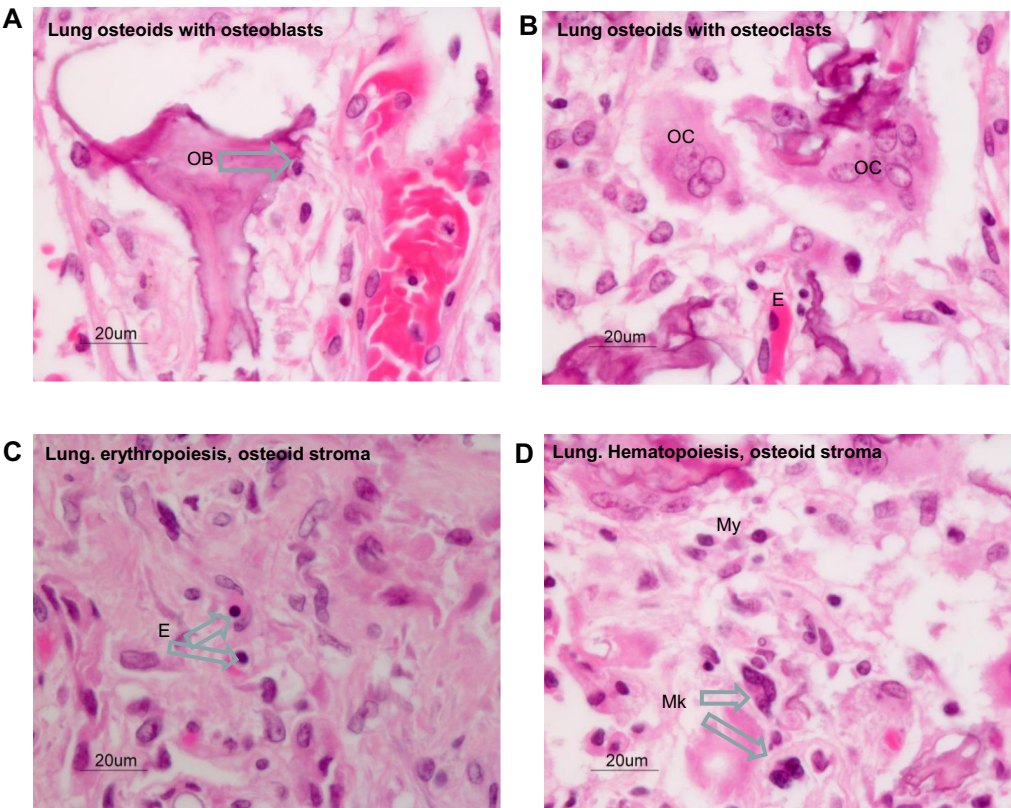D — Lung. Hematopoiesis, osteoid stroma

Figure 4: Hematopoeisis within dendriform ossifications. Osteogenesis and hematopoeisis are present within the pulmonary fibrotic tissues. Bone forming osteoblasts (OB) (panel A) and bone remodeling osteoclasts (OC) (panel B) are associated with the boney trabeculae of the dendriform ossifications; hematopoietic activity is present within the fibrotic osteoid stromal micro-enviroment associated with ossifications. Erythroblasts/normoblasts (E) (panel C) and myeloid precursors (My) and megakaryocytes, mature and immature forms (Mk) (panel D).
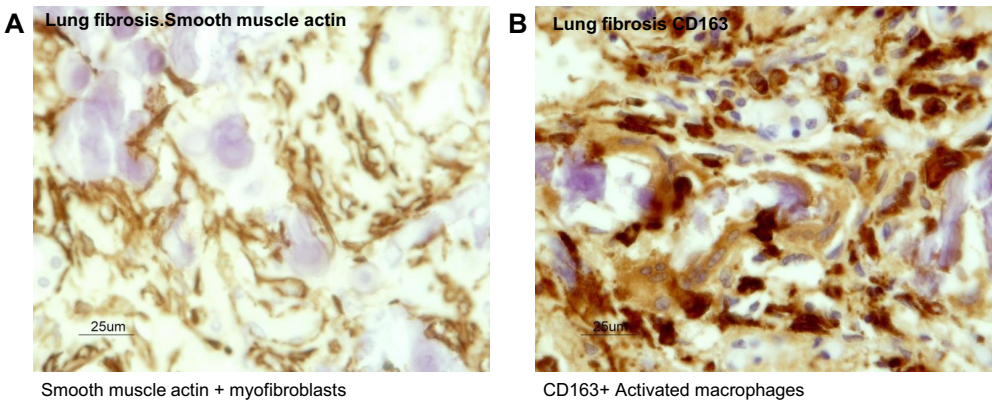

A — Lung fibrosis.Smooth muscle actin — Smooth muscle actin + myofibroblasts

B — Lung fibrosis CD163 — CD163+ Activated macrophages

Figure 5: Lung with honeycomb fibrosis and dendriform diffuse ossification, showing abundant activated macrophages amongst the myofibroblasts and fibroblasts. Lung with honeycomb fibrosis and diffuse dendriform ossification, showing abundant smooth muscle actin expressing fibroblasts and myofibroblasts (A) within the abnormally widened inter-alveolar spaces. Numerous activated macrophages, expressing activation antigen CD163 (B) are amongst these myofibroblasts.

whole genome of the patient was sequenced using the Complete Genomics Inc. (Mountain View, CA) platform.

The resulting sequencing run had >97.5% of the human genome covered by unique reads with depth 5× or greater and >95.7% with depth 10× or greater. The coding
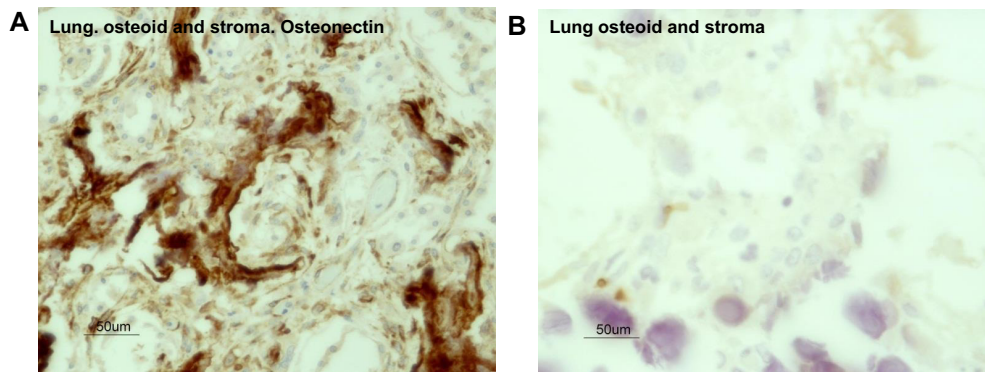
Figure 6: Bone matrix protein osteonectin is expressed by myofibroblasts in micro-environment closely associated within foci of dendriform ossifications. Bone matrix protein is detected in the bone trabeculae as well as the myofibroblasts within the diffuse dendriform ossification micro-environment closely associated within foci of osteogenesis (A). Very few T cells detected by CD3 antibody staining are found within the same areas (B).
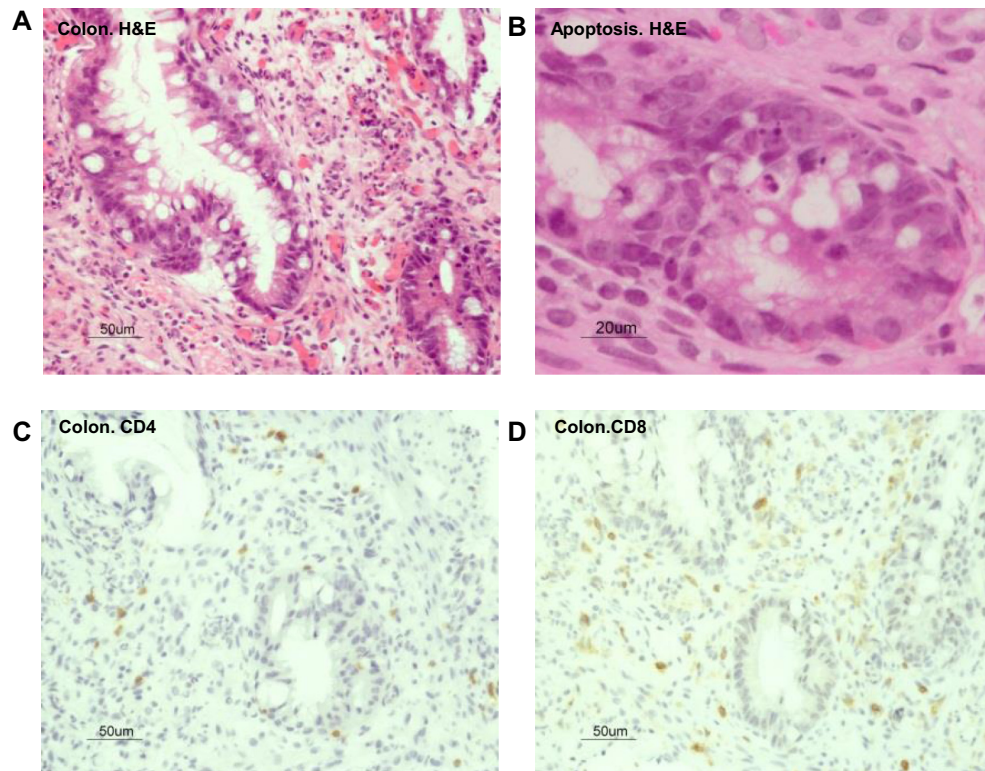

Figure 7: Abnormal features in the intestinal mucosa of the patient. Mucosa shows marked reduction of mucosal gland densities and the glands that remain show crypt distortion (A). No intraepithelial infiltrates of acute inflammatory cells are evident, instead apoptotic enterocytes are seen in unusual locations within the mucosal glandular epithelium such as the crypt base (B). Within the lamina propria, there is a marked reduction of lymphoid cells and immunostains for CD4 helper T cells and CD8 suppressor T cells show marked reduction of CD4 T cell (C) and virtually no CD8 cells (D).

sequence coverage displayed only slightly higher percentages.

Of the 4 656 733 variants that were called (including "half calls" where only one allele is resolved), 4 161 694 (89.4%) passed CGI's default quality filters and 3 776 872 (81.1%) passed the more stringent filters. Of the variants passing quality filters, 24 512 and 22 389 (about 0.6% in both cases) were coding or splicing, respectively; of these, 2758 (11.3%) and 2240 (10%)
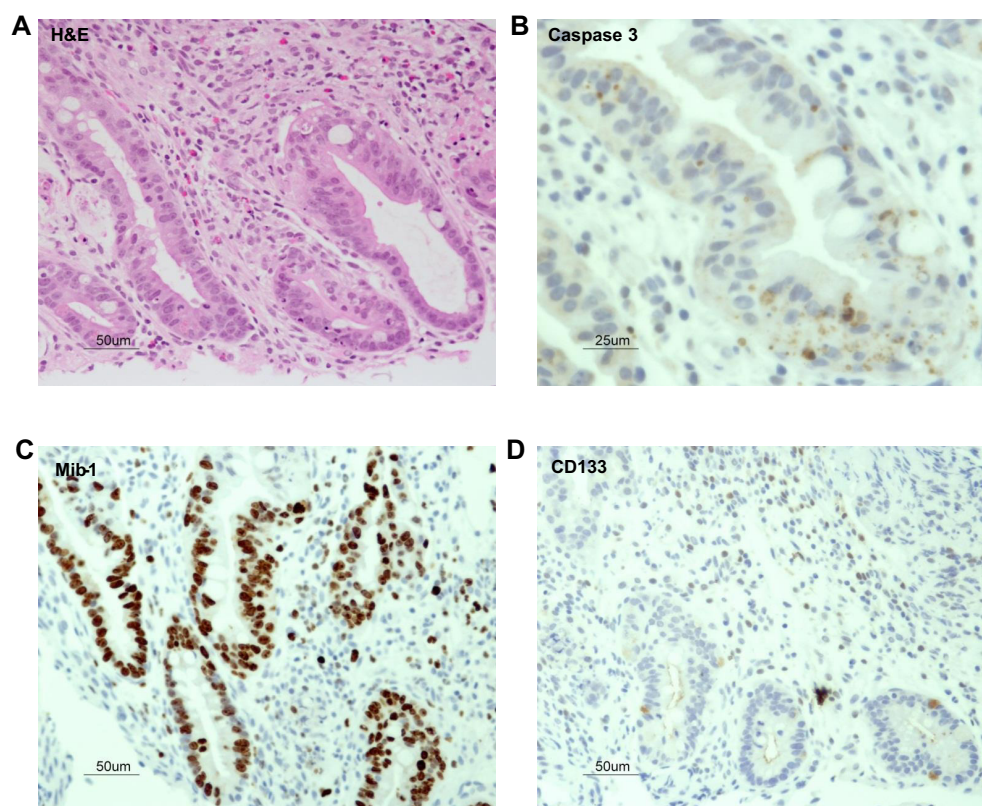
Figure 8: Immunopathological features associated with abnormal intestinal crypt formation. Apoptosis of enterocytes in abnormal crypt locations (A) evidenced by expression of cleaved Caspase 3 (B); marked increase in the transit amplifying zone characterized by Mib-1 positive cells (C); abnormal locations of crypt stem cells detected by CD133 expression (D).

were found to be 5% rare, of which 1595 (6.5%) and 1203 (5.4%) were found to be 1% rare (Figure 9).

Three variants were of high quality, 5% rare, and matched a ClinVar pathogenic record. However, none of them matched a disorder related to the primary immunodeficiency observed in the subject (MSR1, rs72552387: Malignant tumor of prostate, SCN3B, rs121918282: Brugada syndrome 7, HAMP, rs104894696: Hemochromatosis, modifier of).

Two variants were found to be stringent high quality, coding or splicing, 1% rare homozygous, and disrupting a gene product with known immune phenotype association; both were frameshift substitutions, disrupting the genes MMP12 and ZFPM1 (chr11:102738794-102738795, MMP12:NM_002426:exon5:c.630_631AAA; chr16:88599700-88599705, ZFPM1:NM_153813:exon10: c.1334_1339CC). After close inspection, the MMP12 variant was found to be a likely reference sequence error or private variant (based on the HuRef sequence and other mammalian organisms sequence), whereas the

ZPFM1 variants were in a region of dubious coding sequence accuracy.

Although it did not meet the stringent quality requirements, a potential compound heterozygous event was found for CHD4 and was prioritized for follow up because of a particularly interesting phenotype in the mouse model (abnormal T cell counts, hypoplastic thymus, abnormal spleen, liver inflammation); however, validation by Sanger sequencing failed, confirming the importance of focusing on variants with higher quality stringency.

Five variants were found to be stringent high quality, coding or splicing, 1% rare, heterozygous, and disrupting a gene product with known immune and dominant phenotype; however, none of them had clinical presentations compatible with the subject in study (TTN: hypertrophic cardiomyopathy, muscular distrophy; PLEC: epidermolysis bullosa, muscular distrophy; NUP214: acute leukemia; VWF: von Willebrand disease; ITGB3: bleeding disorder, posttransfusion purpura, Glanzmann thrombasthenia).
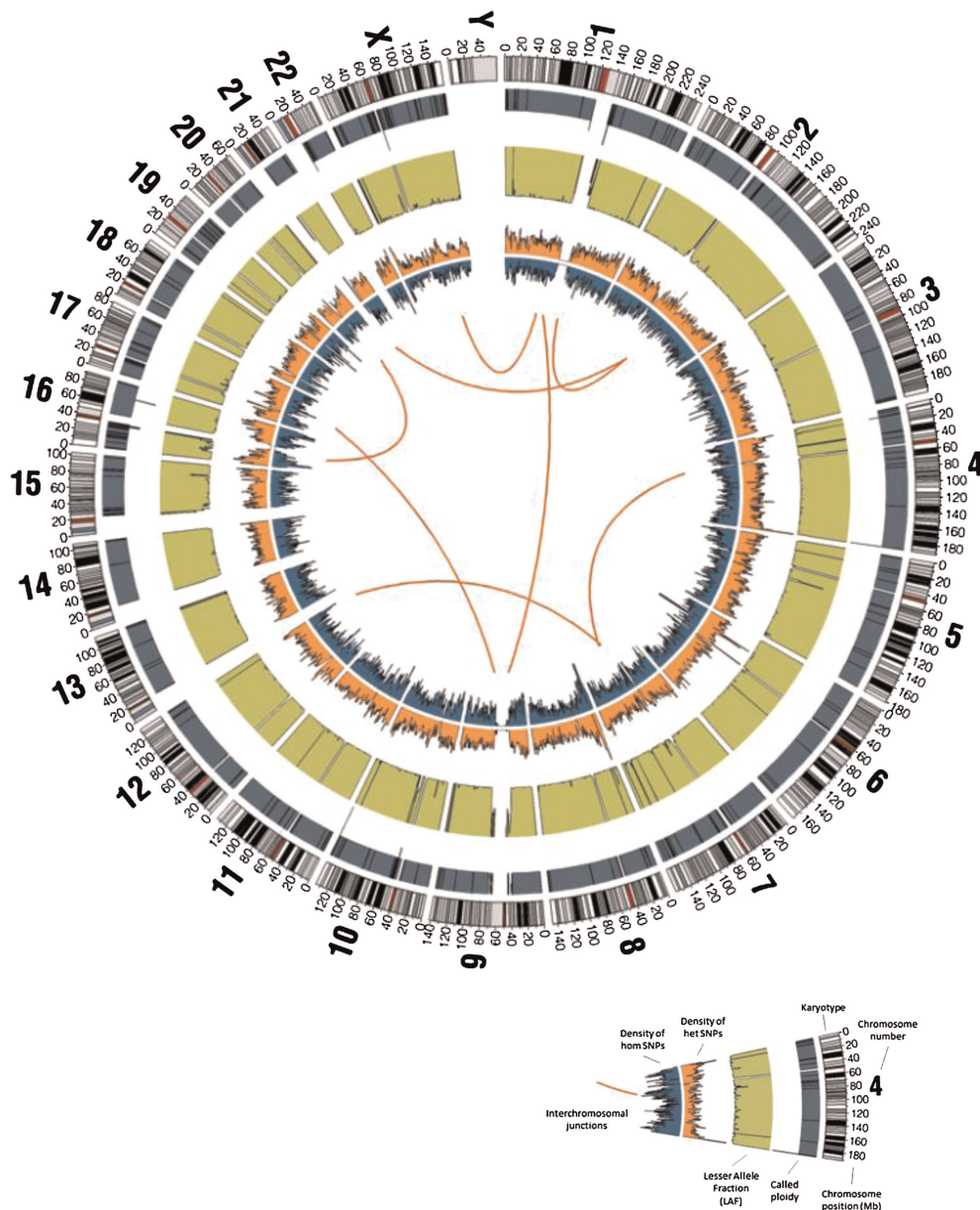
Figure 9: Two heterozygous mutations in the *TTC7A* gene were identified. c:211 G>A (NM 020458.2) (A) resulting in amino acid change E 715K (C). The other mutation was c.1576 C>T (NM 020458.2) (B) resulting in a premature stop codon Q526X (C).

No rare (1%) CNV disrupted more than one gene, and none of the 6 genes with coding exons overlapped by 1% rare losses (*OR5M10*, *FOLH1B*, *TRIM77*, *WFDC8*) or 1% rare gains (*ANKRD36*, *HYDIN*) had any phenotypic or functional information implicating them in the patient's disorder.

Only one gene, *TTC7A,* was found to have a potential compound heterozygous event composed of two or more variants in the stringent high quality group, coding or splicing, 1% rare homozygous, and disrupting a gene product with a known immune phenotype. Interestingly, the OMIM disorder associated with *TTC7A* is intestinal atresia in humans. The two variants, recognized as very low-frequency damaging missense and a novel stop-gain, were inspected carefully and were confirmed to have sufficient damaging potential (*TTC7A*:NM_020458:exon14:c.C1576T: p.Q526X).

Two mutations were confirmed by Sanger sequencing in the patient's and in her parents' *TTC7A* gene. The mother carried a novel heterozygous nonsense mutation in exon 14 c.1576 C > T, a substitution that results in the premature termination of the protein at amino acid 526 (p.Q526X) (Figure 10). The father was
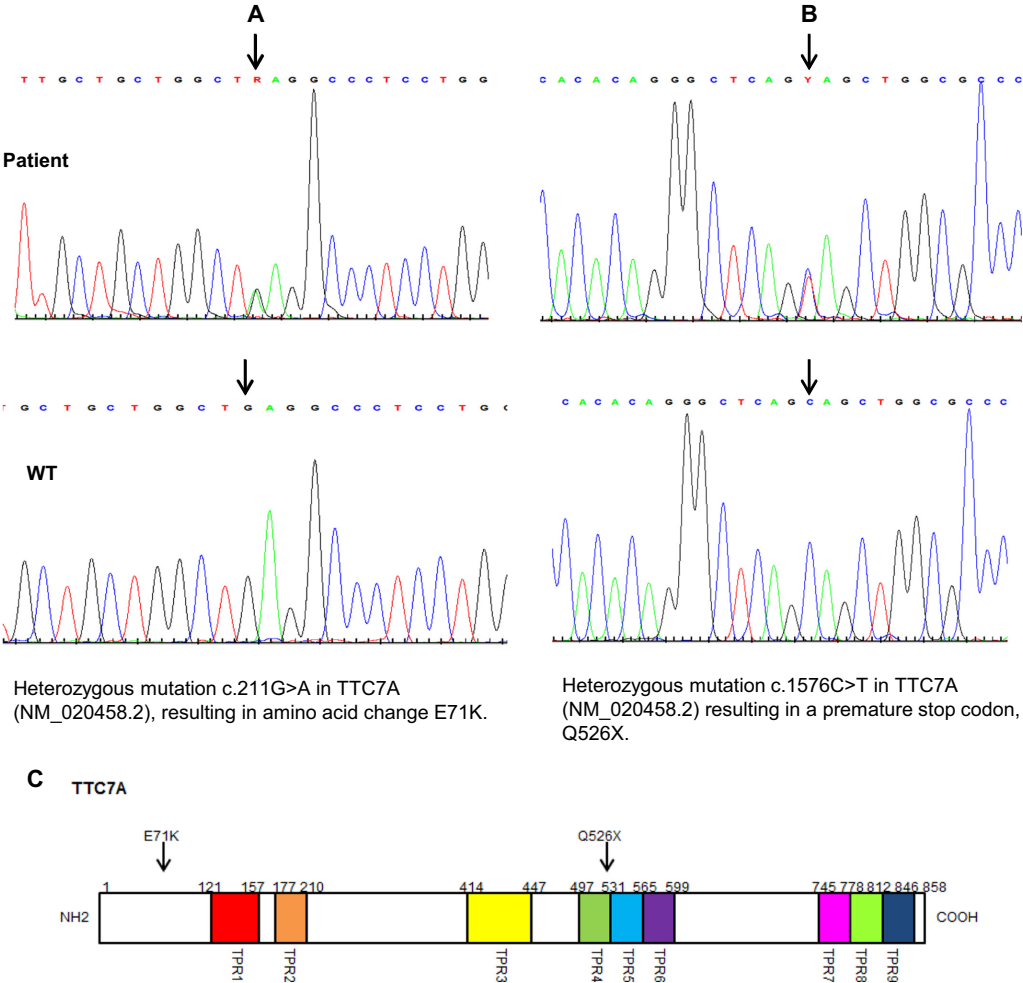
Heterozygous mutation c.211G>A in TTC7A (NM_020458.2), resulting in amino acid change E71K.

Heterozygous mutation c.1576C>T in TTC7A (NM_020458.2) resulting in a premature stop codon, Q526X.

Figure 10: A circos plot showing very limited structural (red lines, centre) alterations, and typically diploid coverage by chromosome (teal track). Regions with lower coverage correspond to centromeres, telomeres, assembly gaps, and other regions that are highly repeat rich and depleted of known coding genes. As expected for a female subject, the X chromosome has diploid coverage whereas the Y chromosome is absent. Heterozygous and homozygous SNP content is very well correlated (orange and blue inner track), suggesting the absence of large-scale homozygosity stretches.

heterozygous for a G to A transition in exon 2 at position 211 (c 211 G > A), which predicts a glutamic acid to lysine substitution at position 71 (p. E71K). This mutation is likely to be deleterious (polyphen score 0.99) and located at the region predicted to be critical for protein–protein interactions (Blatck and Lassle 1992; Scheufler 2000).

Discussion

MIA typically affects both the small intestine and the colon (Mishalany and Der Kaloustian 1971; Guttman et al. 1973; Arnal-Monrea et al. 1983; Moreno et al. 1990; Walker et al. 1993; Gungor et al. 1995; Rothenberg et al. 1995; Moore et al. 1996; Gahukamble et al.

2002; Gahukamble and Gahukamble 2002; Bilodeau et al. 2004; Cole et al. 2010) and is frequently fatal in spite of attempts to surgically correct the lesions (Mishalany and Der Kaloustian 1971; Guttman et al. 1973; Arnal-Monrea et al. 1983; Moreno et al. 1990; Walker et al. 1993; Gungor et al. 1995; Rothenberg et al. 1995; Moore et al. 1996; Gahukamble et al. 2002; Gahukamble and Gahukamble 2002; Bilodeau et al. 2004; Cole et al. 2010). The associated immunodeficiency is variable and the extreme cases present like T^-B^+ SCID or T^+B^+ CID (Mishalany and Der Kaloustian 1971; Guttman et al. 1973; Arnal-Monrea et al. 1983; Moreno et al. 1990; Walker et al. 1993; Gungor et al. 1995; Rothenberg et al. 1995; Moore et al. 1996; Gahukamble et al. 2002; Gahukamble and Gahukamble 2002; Bilodeau et al. 2004; Cole et al. 2010). Several

groups have recently shown that MIA can be associated with mutations in the *TTC7A* gene (Bigorgne et al. 2014; Chen et al. 2013; Samuels et al. 2013).

Little is known about the role of *TTC7A* in the development or function of the immune system. Spontaneous mutations in the mouse *TTC7A* ortholog *Ttc7* results predominantly in a skin disorder reminiscent of psoriasis as well as anemia (Beamer et al. 1995; Abernethy et al. 2000; White et al. 2004; Helms et al. 2005; Takabayashi and Katoh 2005; White et al. 2005; Takabayaski et al. 2007). The flaky skin (*fsn*) mouse results from an insertion of an additional exon between exons 14 and 15, thus leading to an in-frame insertion of 61 amino acids disrupting a TPR domain. This is predicted to be a protein–protein interaction domain likely interacting with components of the cell cycle process, subcellular localization, and phosphorylation events (Beamer et al. 1995; Abernethy et al. 2000; White et al. 2004; Helms et al. 2005; Takabayashi and Katoh 2005; White et al. 2005; Takabayaski et al. 2007). The immune abnormality in the *fsn* mouse is surprisingly mild with some reduction of CD4$^+$ cells and lymphoid hyperplasia (Beamer et al. 1995; White et al. 2004; Helms et al. 2005; Takabayashi and Katoh 2005; White et al. 2005; Abernethy et al. 2000; Takabayaski et al. 2007).

Clearly, the phenotypes of humans and mice affected by mutations in *TTC7* differ vastly. It is unclear whether such differences are species specific or if they are related to the effect of the different mutations. Future studies that elucidate the function of *TTC7A* will no doubt aid in better understanding this discrepancy.

The human cases described to date, had multiple intestinal atresias and various levels of immunodeficiency. The more severely immunologically affected individuals seem to have had severe combined immunodeficiency. Their thymus on autopsy was hypoplastic with reduced cellularity and partial corticomedullarly distinction (Bigorgne et al. 2014; Chen et al. 2013). Similar changes may be related to the underlying condition or possibly caused by stress or consumption of immunosuppressant drugs. However, paucity of Hassall's corpuscles as demonstrated in our case is more likely to be associated with primary immunodeficiency.

The thymus biopsy obtained from our patient showed a clear reduction in the number of Hassall's corpuscles compared with a control, but more importantly, these corpuscles were poorly and only partially formed, indicating a primary immunodeficiency. The lymphopenia, low TRECs and markedly reduced responses to mitogens and antigens were further evidence in support of this notion.

The gut involvement in MIA is interesting and has been studied in depth by several groups (Bigorgne et al. 2014; Avitzur et al. 2014). Pathological features include partial or total villous atrophy with multiple apoptotic figures (Bigorgne et al. 2014) and clear disruption of the epithelial architecture. Intestinal organoid cultures derived from the patients' gut demonstrated inversion of apicobasal polarity of the epithelial cells, a change expected to disrupt growth and differentiation of intestinal epithelial cells (Bigorgne et al. 2014; Avitzur et al. 2014). Similar changes were observed in our patient, yet there was no sign of atresia at any segment of the gut. This may suggest the other factors may be involved in the process of developing atresia. Alternatively, it is possible that some mutations may preserve certain functions of *TTC7A*, thus avoiding formation of atresia.

Diffuse pulmonary ossification is an extremely rare condition. One adult case series review of autopsies performed from 1978–2004, identified only 8 cases from 1393 patients, all were 65 years and older, (Lara et al. 2005). Another review reported an incidence of 1.63 cases per 1000 autopsies (Tseung and Duflou 2006). This condition was initially noted in the literature in 1949, in patients with mitral stenosis (Lawson 1949). Since then, occurrences of this condition were reported to be associated with a variety of lung disorders with a chronic pulmonary disease, with a predilection in males (88%). Histologically, two forms can be distinguished, nodular and dendriform. The former is more commonly associated with passive pulmonary congestion that occurs with mitral valve stenosis, whereas the dendriform type appears associated with chronic lung inflammation (Tseung and Duflou 2006). There is only one report of this condition affecting a father and his son, suggesting a possible hereditary condition (Azuma et al. 2003). However, this condition was never described before in infants.

Recently, myofibroblasts have been implicated in playing an important role in the development of pulmonary fibrosis. These cells can either be derived from the bone marrow, from the resident pulmonary fibroblasts that undergo differentiation, or from the epithelial cells undergoing epithelial mesenchymal

transition. Progression to fibrosis is dependent on proinflammatory and profibrotic mediators, such as transforming growth factor (TGF) β1 (Wynn 2011). Under appropriate induction conditions, fibroblasts and possibly myofibroblasts have been shown to be capable of osteogenic differentiation, evidenced by the expression osteonectin, one of the major noncollagen proteins of bone (Sommar et al. 2013). Osteonectin expression in the myofibroblasts of our patient indicated a direct role of these cells in bone formation in the lung.

In an immunocompetent host, injury to the lung triggers the secretion of interleukin (IL)-25, IL-33, and thymic stromal lymphopoietin (TSLP) from pneumocytes. These mediators can enhance Th2 differentiation and secretion of IL-4 and IL-1, cytokines that can promote secretion of TGF-β1 and other mediators from pro-fibrogenic macrophages as well as recruitment of collagen-secreting macrophages from the bone marrow. TH2 cells can also trigger an antifibrotic feedback process mediated by arginase-1 activity in M2 macrophages, which then inhibit further IL-13 production. Th-1 cells on the other hand that secrete interferon (IFN)-γ can suppress collagen synthesis in fibroblasts by activating M1 macrophages that favor degradation of extracellular matrix (ECM) (Wynn 2011). It is possible therefore that in our patient with CID, increased fibrosis may have been induced by increased profibrotic signals, lack of inhibitory signals, or both.

The intrinsic immunodeficiency in this patient resulted in a high susceptibility to infections and the tissue injuries that follow pulmonary parainfluenza A infection, which could have caused injuries to the alveolar epithelium. This led to release of macrophage-stimulating cytokines that induced proliferation and recruitment fibroblasts/myofibroblasts, which resulted in the development of a fulminant course of pulmonary interstitial fibrosis and fatal respiratory failure.

We report here a unique case of combined immunodeficiency causes by mutations in *TTC7A* without the typical association with MIA. This is also the first description of dendriform lung ossification in an infant.

Acknowledgement

REFERENCES

Abernethy, N.D, Hagan, C., Tan, P.L., Birchall, N.M., and Watson, J.D. 2000. The peripheral lymphoid compartment is disrupted in flaky skin mice. Immunol. Cell Biol. **78**:5–12. PMID: 10651923. doi: 10.1046/j.1440-1711.2000.00866.x.

Arnal-Monrea, F., Pombo, F., and Capdevila-Puerta, A. 1983. Multiple hereditary gastrointestinal atresias: study of a family. Acta. Paediatrica. Scandinavica. **72**:773–777. PMID: 6637476. doi: 10.1111/j.1651-2227.1983.tb09812.x.

Arpaia, E., Shahar, M., Dadi, H., Cohen, A., and Roifman, C.M. 1994. Defective T cell receptor signaling and CD8+ thymic selection in humans lacking Zap-70 kinase. Cell. **76**(5):947–958. PMID: 8124727. doi: 10.1016/0092-8674(94)90368-9.

Avitzur, Y., Guo, C., Mastropaolo, L.A., Bahrami, E., Chen, H., Zhao, Z., et al. 2014. Mutations in Tetratricopeptide Repeat Domain 7A Result in a Severe Form of Very Early Onset Inflammatory Bowel Disease. Gastroenterology, 10 January 2014. pii: S0016-5085(14)00028-6. PMID: 24417819. doi: 10.1053/j.gastro.2014.01.015.

Azuma, A., Miyamoto, H., and Enomoto, T. 2003. Familial clustering of dendriform pulmonary ossification. Sarcoidosis, Vasc. Diffuse. Lung. Dis. **20**:152–154.

Beamer, W.G., Pelsue, S.C., Shultz, L.D., Sundberg, J.P., and Barker, J.E. 1995. The flaky skin (fsn) mutation in mice: map location and description of the anemia. Blood. **86**:3220–3226. PMID: 7579418.

Bigorgne, A.E., Farin, H.G., Lemoine, R., Mahlaoui, N., Lambert, N., and Gil, M., et al. 2014. TTC7A mutations disrupt intestinal epithelial apicobasal polarity. J. Clin. Invest. **124**:328–337. PMID: 24292712.

Bilodeau, A., Prasil, P., Cloutier, R., Laframboise, R., Meguerditchian, A.N., and Roy, G. 2004. Hereditary multiple intestinal atresia: thirty years later. J. Pediat. Surg. **39**:723–730. doi: 10.1016/j.jpedsurg.2004.01.031.

Blatch, G.L., and Lassle, M. 1992. The tetratricopeptide repeat: a structural motif mediating protein-protein interactions. Bioessays. **21**(11):932–939. doi: 10.1002/(SICI)1521-1878(199911)21:11<932::AID-BIES5>3.0.CO;2-N.

Chen, R., Giliani, S., Lanzi, G., Mias, G.I., Lonardi, S., and Dobbs, K., et al. 2013. Whole-exome sequencing

identifies tetratricopeptide repeat domain 7A (TTC7A) mutations for combined immunodeficiency with intestinal atresias. J. Allergy. Clin. Immunol. **132**(2):656–664. PMID: 23830146. doi: 10.1016/j.jaci.2013.06.013.

Cole, C., Freitas, A., Clifton, M.S., and Durham, M. M. 2010. Hereditary multiple intestinal atresias: 2 new cases and review of the literature. J. Pediat. Surg. **45**:E21–E24. PMID: 20385266.

Gahukamble, D.B., and Gahukamble, L.D. 2002. Multiple gastrointestinal atresias in two consecutive siblings. Pediat. Surg. Int. **18**:175–177. PMID: 11956791. doi: 10.1007/s003830000536.

Gahukamble, D.B., Adnan, A.R., and Al-Gadi, M. 2002. Atresias of the gastrointestinal tract in an inbred, previously unstudied population. Pediat. Surg. Int. **18**:40–42. PMID: 11793062. doi: 10.1007/s003830200009.

Gungor, N., Balci, S., Tanyel, F.C., and Gogus, S. 1995. Familial intestinal polyatresia syndrome. Clin. Genet. **47**:245–247. PMID: 7554349. doi: 10.1111/j.1399-0004.1995.tb04304.x.

Guttman, F.M., Braun, P., Garance, P.H., Blanchard, H., Collin, P.P., and Dallaire, L. 1973. Multiple atresias and a new syndrome of hereditary multiple atresias involving hastrointestinal tract from stomach to rectum. J. Pediat. Surg. **8**:633–640. PMID: 4752999. doi: 10.1016/0022-3468(73)90401-6.

Helms, C., Pelsue, S., Cao, L., Lamb, E., Loffredo, B., and Taillon-Miller, P., et al. 2005. The tetratricopeptide repeat domain 7 gene is mutated in flaky skin mice: a model for psoriasis, autoimmunity and anemia. Exp. Biol. Med. **230**:659–667. PMID: 16179734.

Lara, J.F., Catroppo, J.F., and Kim, D.U. 2005. Dendriform pulmonary ossification, a form of diffuse pulmonary ossification: report of 26 year autopsy study experience. Arch. Pathol. Lab. Med. **129**:348–353. PMID: 15737029.

Lawson, H.M. 1949. Disseminated ossification of the lungs of association with mitral stenosis. Br. Med. J. **1**:433. PMID: 18113813. doi: 10.1136/bmj.1.4601.433.

Mishalany, H.G., and Der Kaloustian, V.M. 1971. Familial multiple-level intestinal atresias: report of two siblings. J. Pediat. **79**:124–125. PMID: 5091250. doi: 10.1016/S0022-3476(71)80072-0.

Moore, S.W., de Jongh, G., Bouic, P., Brown, R.A., and Kirsten, G. 1996. Immune deficiency in familial duodenal atresia. J. Pediat. Surg. **31**:1733–1735. PMID: 8987005. doi: 10.1016/S0022-3468(96)90066-4.

Moreno, L.A., Gottrand, F., Turck, D., Manouvrier-Hanu, S., Mazingue, F., and Morisot, C. 1990. Severe combined immunodeficiency syndrome associated with autosomal recessive familial multiple gastrointestinal atresias: study of a family. Am. J. Med. Genet. **37**:143–146. doi: 10.1002/ajmg.1320370133.

Roifman, C.M., Somech, R., Kavadas, F., Pires, L., Nahum, A., Dalal, I., and Grunebaum, E. 2012. Defining Combined Immunodeficiency. J. Allergy. Clin. Immunol. **130**(1):177–183. PMID: 22664165. doi: 10.1016/j.jaci.2012.04.029.

Sharfe, N., Shahar, M., and Roifman, C.M. 1997. An interleukin-2 receptor gamma chain mutation with normal thymus morphology. J. Clin. Invest. **100**(12):3036–3043. PMID: 9399950. doi: 10.1172/JCI119858.

Roifman, C.M., and Dadi, H.K. 2000. Human Interleukin-2 receptor a deficiency. *In* Primary T cell Immunodeficiencies. Immunology, Allergy Clinics of North America. WB Saunders Company, Pennsylvania.

Rothenberg, M.E., White, F.V., Chilmonczyk, B., and Chatila, T. 1995. A syndrome involving immunodeficiency and multiple intestinal atresias. Immunodeficiency. **5**:171–178. PMID: 7749436.

Samuels, M.E., Majewski, J., Alirezaie, N., Fernandez, I., Casals, F., and Patey, N., et al. 2013. Exome sequencing identifies mutations in the gene TTC7A in French-Canadian cases with hereditary multiple intestinal atresia. J. Med. Genet. **50**:324–329. PMID: 23423984. doi: 10.1136/jmedgenet-2012-101483.

Scheufler, C. 2000. Structure of TPR domain-peptide complexes: critical elements in the assembly of the Hsp70-Hsp90 multichaperone machine. Cell. **101**(2):199–210. PMID: 10786835. doi: 10.1016/S0092-8674(00)80830-2.

Sommar, P., Junker, J.P., and Strandenes, E. 2013. Osteogenically induced human dermal fibroblasts as a tool to regenerate bone. J. Plast. Surg. Hand. Surg. **47**:8–13. PMID: 23327789. doi: 10.3109/2000656X.2012.731411.

Takabayaski, S., Iwashita, S., Hirashima, T., and Katoh, H. 2007. The novel tetratricopeptide repeat domain 7 mutation, Ttc7fsn-Jic, with deletion of the TPR-SB repeat causes severe flaky skin phenotype. Exp. Biol. Med. **323**:695–699.

Tseung, J., and Duflou, J. 2006. Diffuse pulmonary ossification: an uncommon incidental autopsy finding. Pathology. **38**:454–458. PMID: 17008289. doi: 10.1080/00313020500464912.

Walker, M.W., Lovell, M.A., Kelly, T.E., Golden, W., and Saulsbury, F.T. 1993. Multiple areas of intestinal atresia associated with immunodeficiency and posttransfusion graft-versus-host disease. J. Pediat. **123**:93–95. PMID: 8320633. doi: 10.1016/S0022-3476(05)81547-1.

Takabayashi, S., and Katoh, H. 2005. A mutant mouse with severe anemia and skin abnormalities controlled by a new allele of the flaky skin (fsn) locus. Exp. Anim. **54**:339–347. PMID: 16093647. doi: 10.1538/expanim.54.339.

Wang, K., Li, M., and Hakonarson, H. 2010. ANNOVAR: functional annotation of genetic variants from high-throughput sequencing data. Nucl. Acid. Res. **38**:164. doi: 10.1093/nar/gkq603.

White, R.A., McNulty, S.G., Nsumu, N.N., Boydston, L.A, Brewer, B.P., and Shimizu, K. 2005. Positional cloning of the Ttc7 gene required for normal iron homeostasis and mutated in hea and fsn anemia mice. Genomics. **85**:330–337. PMID: 15718100. doi: 10.1016/j.ygeno.2004.11.008.

White, R.A., McNulty, S.G., Roman, S., Garg, U., Wirtz, E., and Kohlbrecher, D., et al. 2004. Chromosomal localization, hematologic characterization, and iron metabolism of the hereditary erythroblastic anemia (hea) mutant mouse. Blood. **104**:1511–1518. PMID: 15155459. doi: 10.1182/blood-2004-01-0076.

Wynn, T.A. 2011. Integrating mechanisms of pulmonary fibrosis. J. Exp. Med. **208**:1339–1350. PMID: 21727191. doi: 10.1073/pnas.092134099.